Branching Fractions and Transition Probabilities for UV Transitions in the Spectrum of Cr ii

Ward, J.W.; Li, J. J.; Schwartz, J.; Nave, G.; Raassen, T.A.J.J.; Uylings, P.H.M.

DOI
10.3847/1538-4357/acfafe

Publication date
2023

Document Version
Final published version

Published in
Astrophysical Journal

The Astrophysical Journal, 959:8 (11pp), 2023 December 10 https://doi.org/10.3847/1538-4357/acfafe

Branching Fractions and Transition Probabilities for UV Transitions in the Spectrum of Cr II

Jacob W. Ward[1,2], Jacqueline J. Li[1,3], Jared Schwartz[2], Gillian Nave[1], Ton A. J. J. Raassen[4,5], and Peter H. M. Uylings[4]
[1] National Institute of Standards and Technology, Gaithersburg, MD 20899-8422, USA
[2] University of Maryland College Park, College Park, MD 20742, USA
[3] University of Pennsylvania, Philadelphia, PA 19104, USA
[4] Anton Pannekoek Institute for Astronomy, University of Amsterdam, The Netherlands
[5] SRON Netherlands Institute for Space Research, Utrecht, The Netherlands
Received 2022 November 30; revised 2023 September 8; accepted 2023 September 10; published 2023 November 28

Abstract

We present transition probabilities for 268 spectral lines of singly ionized chromium (Cr II) in the wavelength region 208–414 nm. Branching fractions were measured in archival Fourier transform spectra of chromium-argon and chromium-neon hollow cathode lamps and a Penning discharge source. The branching fractions were combined with previously published experimental lifetimes of 14 levels, and with lifetimes from semiempirical calculations for 14 levels to give transition probabilities. The estimated uncertainties of the transition probabilities range from 10% to 26%. A comparison with previously published experimental transition probabilities shows discrepancies of up to a factor of 2.5 for lines around 213 nm.

Unified Astronomy Thesaurus concepts: Atomic spectroscopy (2099); Transition probabilities (2074); Atomic data (2216)

Supporting material: machine-readable table, data behind figures

1. Introduction

The high cosmic abundance and rich spectra of iron-group elements mean that they are important contributors to the spectra of a wide variety of objects, including the photospheres of the Sun, A and B-type stars, the chromospheres of cooler stars, the interstellar medium, quasars, and absorption spectra in galaxies and interstellar clouds. Iron-group elements are so dominant in the spectra of many A- and B-type stars that it is nearly impossible to perform an abundance analysis of any other element without accurate atomic data for iron-group elements. In the ultraviolet (UV) region, high-resolution spectra with a high signal-to-noise (S/N) ratio have been the focus of several programs with the Hubble Space Telescope, including spectra of both hot and cool stars, to provide high-quality reference data over a wide wavelength region and to complement spectra from ground-based telescopes. A successful abundance analysis of these spectra requires comprehensive atomic data, as shown in the analysis of HR 6000 by Castelli et al. (2017). In some cases, the abundance analysis can only be carried out in the UV region, where key lines of the most abundant ionization stage are found, which is the singly ionized stage for iron-group elements. These key lines are particularly valuable when probing non–local thermodynamic equilibrium effects in stars (Lawler et al. 2017a).

However, the measurement of accurate transition probabilities in the UV region poses several difficulties. The most common laboratory technique combines the measurement of the lifetime, τ_k, of an upper energy level, k, using laser-induced fluorescence with a separate measurement of the branching fractions (BFs). The BF, BF_{ki}, of a transition from upper level, k, to lower level, i, is defined as

$$BF_{ki} = A_{ki} \Big/ \sum_j A_{kj} = A_{ki}\tau_k \quad (1)$$

where A_{ki} is the transition probability in s^{-1}. It can be determined from the relative intensity of spectral lines in experimental emission spectra, using

$$BF_{ki} = I_{ki} \Big/ \sum_j I_{kj} \quad (2)$$

where I_{ki} is the intensity of the line in units of photons s^{-1}. In both equations, the sums are over all transitions from the upper energy level, k.

In the UV region, many lines of interest originate from high energy levels that are difficult to reach with standard laboratory lasers suitable for lifetime measurements. In addition, their lifetimes are often only a few nanoseconds, which is close to the pulse length of lasers usually used for these lifetime measurements. Hence there are many more measured lifetimes for neutral iron-group spectra than for singly ionized iron-group spectra. The measurement of BFs in the UV region also poses problems with the radiometric calibration of the spectra, as it is often necessary to use more than one radiometric standard lamp to cover the full set of decays from an upper level. These problems were addressed in Lawler et al. (2017b), where a significant effort was needed to confirm the radiometric calibration of Cr II lines in the near-UV region. These techniques included the comparison of the branching ratios, BR_{kij}, of two lines with the common upper level, k, and lower levels, i and j, in different spectra where

$$BR_{kij} = A_{ki}/A_{kj} = I_{ki}/I_{kj}. \quad (3)$$

In this paper, we present BFs for 268 lines of singly ionized chromium covering the wavelength range 208–414 nm. We convert them to transition probabilities using both experimental and calculated lifetimes. Roughly 125 of these are new

measurements of lines originating from the $(a^3P)4p\,y\,^4D$, $(a^3F)4p\,z\,^4G$, $(^3H)4p\,z\,^4I$, and $(^3H)4p\,z\,^2G$ terms with energy level values from 63,801 to 65,813 cm^{-1}.

1.1. Previous Measurements of Cr II Transition Probabilities

The transition probabilities displayed in the National Institute of Standards and Technology (NIST) Atomic Spectra Database (ASD) (Kramida et al. 2022) are based on the compilation of Fuhr & Wiese (2005), which contains experimental transition probabilities for 92 lines of Cr II, of which 49 lie in the UV region below 400 nm. The majority of these UV lines are taken from Musielok & Wujec (1979), who measured absolute intensities in an arc source. The uncertainty grade of these lines in ASD is "D," corresponding to better than 50%. Eight lines in ASD were taken from the compilation of Morton (2003), who combined BF measurements of Bergeson & Lawler (1993) with lifetime measurements from Schade et al. (1990), Pinnington et al. (1993), and Bergeson & Lawler (1993). Three of the eight lines have a grade of "B+" in ASD, corresponding to a 7% uncertainty. The other five lines have no assigned uncertainty in ASD.

Since the compilation of Fuhr & Wiese (2005), experimental Cr II transition probabilities covering the UV region have been published by Nilsson et al. (2006), Gurell et al. (2010), Engström et al. (2014), and Lawler et al. (2017b). All four of these studies combined measurements of lifetimes using time-resolved laser-induced fluorescence (TRLIF) with BFs measured using Fourier Transform (FT) spectroscopy. The Nilsson et al. (2006) and Lawler et al. (2017b) papers focused on levels of the $3d^4(^5D)4p$ configuration in the energy range 48,500–55,000 cm^{-1}, giving spectral lines in the wavelength region from 250 to 642 nm. The work of Engström et al. (2014) covered transitions from the $3d^4(a\,^5D)5s\,e\,^6D$ term at energies of around 83,000 cm^{-1}. The work of Gurell et al. (2010) covered 14 levels in between these two energy regions from the $3d^4(a\,^3H)4p$ and $3d^4(a\,^3F)4p$ configurations between 63,600 and 67,400 cm^{-1}, with 34 lines below 250 nm. Our current work is motivated by the need to both confirm the work of Gurell et al. (2010) and extend the analysis to other levels giving spectral lines in this wavelength region.

Recent theoretical calculations of transition probabilities include Raassen & Uylings (1996), Kurucz (2016), Bouazza et al. (2018a, 2018b), and Tayal & Zatsarinny (2020). The calculations of Bouazza et al. (2018a) focus on highly excited $3d^4\,5s$ levels and those of Bouazza et al. (2018b) on low-lying $3d^4\,4p$ levels. Both papers focus on levels with previous experimental lifetime measurements. The calculations of Raassen & Uylings (1996), Kurucz (2016), and Tayal & Zatsarinny (2020) are more extensive and cover levels that have no experimental lifetime measurements. We have redone the semiempirical calculations of Raassen & Uylings (1996) with the new and updated energy levels of Sansonetti & Nave (2014), and compare them with the calculations of Kurucz (2016) and Tayal & Zatsarinny (2020) in Section 4.1.

The measurement of transition probabilities using experimental or theoretical lifetimes and branching fractions from FT spectroscopy relies on accurate wavelengths, energy levels, and line identifications from previous work. The most recent study of the spectrum of Cr II was that of Sansonetti et al. (2012) and Sansonetti & Nave (2014). These two papers increased the number of known Cr II lines by a factor of over 4 and decreased the energy level uncertainties by a factor of over 20. Both of these improvements are important for accurate BF measurements, which rely on identifying all transitions from a particular upper level. If accurate energy levels are available, they can be used to determine the intensities of individual transitions in a blend, as we describe in Section 4.3.

2. Experimental Methods

The approach to measuring transition probabilities we use in this work is detailed in Section 2 of Kling & Griesmann (2000). The method combines BFs derived from accurate measurements of calibrated line intensities with measured or calculated level lifetimes to generate transition probabilities. In the UV region it is experimentally difficult to measure accurate level lifetimes, but Gurell et al. (2010) report radiative level lifetimes for 14 odd levels of Cr II measured using TRLIF. When experimental values are not available, as is the case for roughly half of the levels in our work, it is possible to use semiempirical calculations. The accuracy of the measured and calculated lifetimes we use and their impact on the uncertainties of the resulting transition probabilities is discussed in Section 4.1.

The experimental arrangement used to record the BFs is described in detail in Kling & Griesmann (2000). Table 1 shows the archival spectra that were used for their measurement. Spectra 1 through 7 were recorded by Ulf Griesmann and Andreas Knoche using the NIST vacuum ultraviolet FT spectrometer (Griesmann et al. 1999) at resolutions of 0.033–0.1 cm^{-1}. The source for spectra 1 through 6 was a high-current hollow cathode lamp (HCL) with a pure chromium cathode (Danzmann et al. 1988). The source for spectrum 7 was a Penning discharge lamp with pure chromium cathodes (Heise et al. 1994). Spectrum 9 was recorded with a commercial Cr/Ne HCL at a current of 20 mA using the same spectrometer. Spectrum 8, of a high-current HCL, was recorded using the NIST 2-m UV-visible-IR FT spectrometer and was used in the analysis of the spectrum of Cr II (Sansonetti & Nave 2014). Spectra 3, 7, and 8 were also used in the measurement of visible-UV transition probabilities by Lawler et al. (2017b).

Each spectrum was calibrated using the spectrum of a radiometric standard lamp taken at the same time as the chromium spectrum. The use of archival spectra in the present analysis posed two challenges in the radiometric calibration of the spectra, as the calibration spectrum for spectrum number 7 was damaged and the original calibration of deuterium lamp BR0065 was missing. The missing calibration is not a serious problem, because deuterium lamps have very similar relative radiances in the wavelength region from 200 to 400 nm, provided that they are of similar construction and have the same window. We compared a frequently used deuterium lamp with a MgF_2 window, V0236, with a rarely used one, V0194, and found that they agreed within 3% over the wavelength range 166–390 nm. We thus applied the calibration of lamp BQ0057 to lamp BR0065, assigning an additional uncertainty of 3% for the transfer of the calibration. This assumption was verified by comparing BRs of strong Cr II lines in spectra 1 and 2, calibrated with BQ0057, with those in spectra 3 through 6, calibrated with BR0065.

Spectrum 7 was the only spectrum recorded of a Penning discharge lamp. It is a valuable spectrum due to its higher S/N ratio and because the different source conditions can point to problems with line blends, particularly blends with Cr I lines that are very weak in the Penning spectrum. However, the

Table 1
Table of Spectra

ID	Date	Wavelength Range (nm)	Wavenumber (cm^{-1})	Coadds	Resolution (cm^{-1})	Gas	Pressure (Pa)	Current (A)	Detector	Calibration Lamp	Comments
1	2000 Oct 27 #1	183 to 317	31,500 to 54,600	64	0.08	Ar	80	0.7	R7154	D_2 # BQ0057	HCL[a]
2	2000 Oct 27 #3	183 to 317	31,500 to 54,600	64	0.08	Ar	85	1.5	R7154	D_2 # BQ0057	HCL[a]
3	2000 Nov 06 #1	249 to 400	25,000 to 40,100	64	0.033	Ar	85	0.7	R106UH	D_2 # BR0065	HCL[a] 11[b]
4	2000 Nov 06 #3	183 to 320	31,200 to 54,600	128	0.09	Ar	85	1.5	R7154	D_2 # BR0065	HCL[a]
5	2000 Nov 07 #1	183 to 317	31,500 to 54,600	128	0.06	Ar	85	1.5	R7154	D_2 # BR0065	HCL[a]
6	2000 Nov 07 #2	183 to 317	31,500 to 54,600	64	0.06	Ar	85	0.7	R7154	D_2 # BR0065	HCL[a]
7	2000 Dec 08 #1	183 to 322	31,000 to 54,600	128	0.15	Ne	0.4	1.4	R7154	None	Penning 17[b]
8	2011 Jun 10 #7	285 to 1207	8280 to 35,000	107	0.02	Ne	400	2	diode	W lamp IR456	HCL[a] 18[b]
9	2016 Apr 24 #5	190 to 704	14,200 to 52,500	259	0.1	Ne	…[c]	0.02	R106UH & R636-10	D_2 #V0236 & W #IR456	HCL

Notes.
[a] HCL: high-current hollow cathode lamp.
[b] Number of spectrum in Table 2 of Lawler et al. (2017b).
[c] Spectrum 9 was of a commercial Cr/Ne hollow cathode lamp and the gas pressure is unknown.

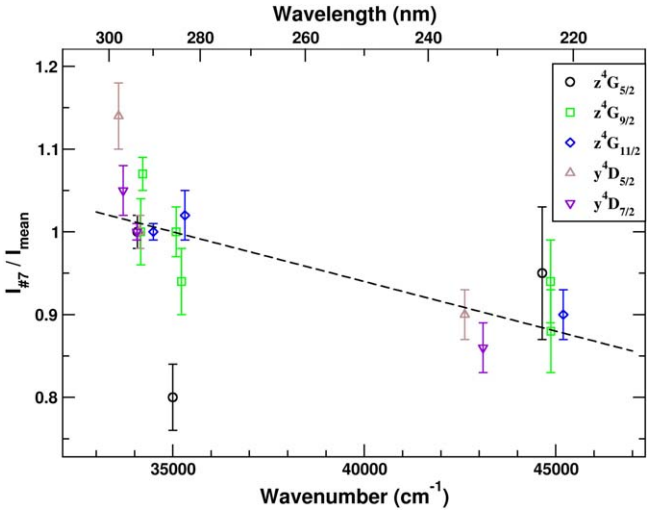

Figure 1. Comparison of the intensity of strong lines from five levels of the z^4G and y^4D terms in Cr II in spectrum 7, $I_{\#7}$, to the weighted mean intensity, I_{mean}, of the same line in spectra 1–6, 8, and 9 in Table 1. The line intensities in each spectrum from each upper level were scaled so that the line nearest 34,000 cm^{-1} from each upper energy level had an intensity of 1. The dashed line shows the 15% change in response between 35,000 and 45,000 cm^{-1} that was used to derive the correction to the response derived from spectrum 6. The error bars represent one standard uncertainty. The line intensities and wavenumbers used to create this plot are available as data behind the figure in the online version of this article.

(The data used to create this figure are available.)

calibration file for this run was damaged. To calibrate spectrum 7, we used the calibration for spectrum 6, which covered a similar wavelength range. Since it is likely that the response of the FT spectrometer had changed between recording spectra 6 and 7, we compared the intensity of strong Cr II lines in spectrum 7, with the mean line intensity of the same line in spectra 1, 6, 8, and 9, as shown in Figure 1. The intensities of the lines from each upper level in each spectrum were scaled so that the line nearest 34,000 cm^{-1} from each energy level had an intensity of 1. An accurate initial calibration would then show no slope and all points on the plot would have a value of 1. The figure shows a 15% change in the response of the FT spectrometer between 35,000 and 45,000 cm^{-1} between the two runs, derived from an unweighted linear fit. This was applied as a correction to the calibration derived from spectrum 6, giving good consistency in the BRs. Since the relative line intensities in Figure 1 could not confirm the calibration outside the region 32,000–45,000 cm^{-1}, the results from spectrum 7 were restricted to this region.

Spectrum 9 was recorded specifically for verifying the radiometric calibrations of other spectra in the UV and visible regions, and the low current also helps to detect any problems with self-absorption in strong Cr II lines. It was calibrated with both deuterium and tungsten standard lamps to cover the region from 17,000 to 50,000 cm^{-1}.

3. Theory

Experimental lifetimes are unavailable for half of the levels for which we have measured BFs. Measurements of lifetimes of high-excitation levels in iron-group elements are difficult to perform and there are few experimental spectroscopy groups capable of performing such measurements. It is thus necessary to use alternate methods to convert our branching fractions into transition probabilities. In this work, we use lifetimes from semiempirical calculations for converting our BFs to transition probabilities. These are derived by taking the inverse of the sum of the calculated transition probabilities from all decays from the upper level. The lifetimes are dominated by the strongest lines emitted from the upper level and these can generally be calculated with the lowest uncertainties. In contrast, weaker lines tend to have larger uncertainties in the calculations as they may be affected by cancellation effects. We justify this assumption in Section 4.4 by comparing the experimental and calculated BFs. Two sets of calculations are compared to derive the lifetimes: the calculations of Kurucz (2016) using the Cowan code, and calculations two of us have performed using the orthogonal operator method (Uylings & Raassen 2019). The uncertainty of the calculate lifetimes for the new levels is derived by comparing calculated lifetimes with previous experimental values, as described in Section 4.1.

Table 2
Values for the Electric Dipole Transition Integrals for Cr II in Atomic Units Calculated by Means of MCDHF Including Core Polarization

Cr II	3d^{4}4p	3d^{3}4s4p	3d^{2}4s^{2}4p	3d^{4}5p	3d^{4}4f	3d^{4}6p
3d^5	1.05	⋯	⋯	0.23	0.36	0.13
3d^{4}4 s	−2.91	0.83	⋯	0.06	⋯	0.07
3d^{3}4s^2	⋯	−2.71	0.67	⋯	⋯	⋯
3d^{4}4d	−3.44	⋯	⋯	5.16	−6.05	0.24
3d^{4}5 s	2.13	⋯	⋯	−6.73	⋯	−0.14
3d^{4}5d	−0.84	⋯	⋯	−6.32	6.80	10.46
3d^{4}6 s	0.59	⋯	⋯	4.88	⋯	−11.72

Transition probability calculations of complex systems such as Cr II require highly accurate eigenvectors. Therefore a semiempirical approach, in which parameters of a model Hamiltonian are adjusted to yield eigenvalues as closely as possible to the experimental energies taken from Sansonetti & Nave (2014), seems a logical choice. In this work we use the orthogonal operator method (Hansen et al. 1988; Uylings & Raassen 2019) that ensures least correlation between the operators and thereby more stability in the fit, even for small configuration interactions.

The even parity model space is extended to seven configurations: 3d^5 + 3d^{4}4 s + 3d^{3}4s^2 + 3d^{4}4d + 3d^{4}5 s + 3d^{4}5d + 3d^{4}6 s with a standard deviation of 4.9 cm^{-1} for the lowest three configurations and an overall $\sigma = 46.6$ cm^{-1}. Similarly, the odd parity model space is build from six configurations: 3d^{4}4p + 3d^{3}4s4p + 3d^{2}4s^{2}4p + 3d^{4}5p + 3d^{4}4f + 3d^{4}6p with an estimated standard deviation of 15 cm^{-1} for the lowest two configurations and an overall $\sigma = 41.5$ cm^{-1}. To calculate A-values, the resulting eigenvectors of the even and odd system are used, in combination with radial electric dipole transition integrals (listed in Table 2) taken from relativistic Hartree–Fock MCDHF calculations (Froese Fischer et al. 2019).

4. Analysis and Results

The basic method of obtaining transition probabilities from measurements of lifetimes and BFs is described in Kling & Griesmann (2000). The BFs measured in the spectra listed in Table 1 were analyzed using the XGREMLIN program (Nave et al. 2015). XGREMLIN was used to both estimate the background noise of the spectrum and to fit the measured lines with Voigt profiles so that the lines could be identified

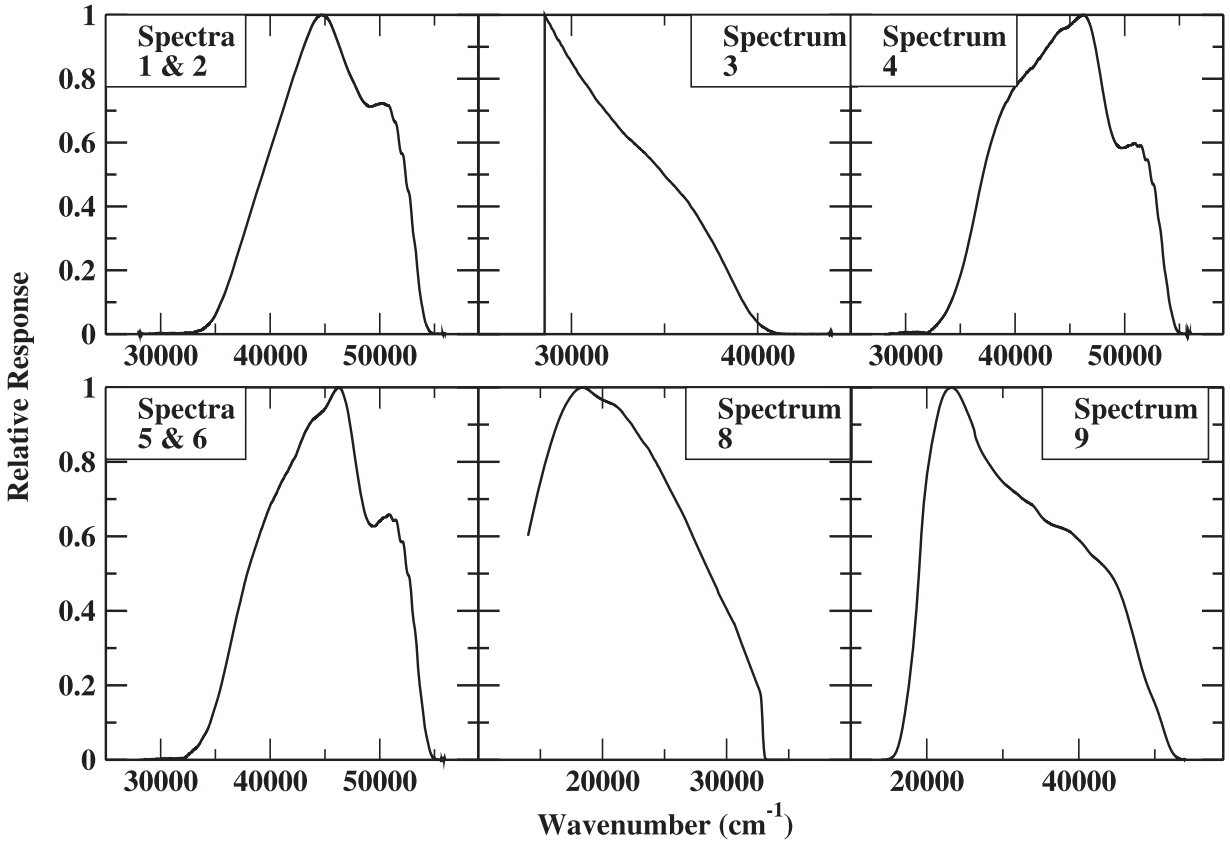

Figure 2. Relative response of the spectrometer for the spectra in Table 1. The response curve for spectrum 7 is not shown, but was derived from the response curve for spectra 5 and 6 as described in Section 2 and Figure 1. Irregularities in the response curves at wavenumbers greater than 50,000 cm^{-1} are caused by air in the path between the source and the spectrometer and BFs were thus not calculated in this region.

Table 3
Comparison of Experimental and Semiempirical Lifetimes for Some Levels of the $3d^4 4p$ Configuration

Term	J	Level Value[a] (cm^{-1})	Exp.[b] Lifetime (ns)	Unc.[c] (ns)	Kurucz[d] Lifetime (ns)	This Work[e] Lifetime (ns)	Residual[f] (%)
$(^3H)4p\ z\ ^4H°$	7/2	63,600.8606	4.4	0.4	4.3	4.4	0.9
	9/2	63,706.2511	4.4	0.4	4.3	4.4	1.2
	11/2	63,848.6962	4.2	0.3	4.3	4.4	0.5
	13/2	64,030.5053	4.2	0.3	4.2	4.3	0.1
$(a^3F)4p\ y\ ^4F°$	3/2	67,070.4394	3.9	0.5	4.1	4.4	5.9
	5/2	67,012.0754	3.7	0.4	3.9	4.2	11.5
	7/2	67,393.4495	2.9	0.2	2.7	2.8	3.4
	9/2	67,448.5405	2.9	0.2	2.9	2.9	3.7
$(^3H)4p\ y\ ^4G°$	5/2	67,344.0068	2.6	0.2	2.3	2.5	3.0
	7/2	67,333.7774	2.6	0.2	2.5	2.5	2.3
	9/2	67,353.2671	2.6	0.2	2.4	2.5	1.5
	11/2	67,369.0687	2.7	0.2	2.4	2.5	1.1
$(a^3F)4p\ z\ ^2D°$	3/2	67,379.295	3.1	0.3	3.4	3.3	6.8
	5/2	67,387.0906	3.1	0.3	3.7	3.2	7.6

Notes.
[a] Experimental energy level value from Sansonetti & Nave (2014).
[b] Experimental lifetime from Gurell et al. (2010).
[c] One standard uncertainty of the experimental lifetime.
[d] Calculated lifetime from Kurucz (2016).
[e] Calculated lifetime from the present work.
[f] Sum of BFs for all calculated lines that were not observed in our spectra.

with a known transition and given an estimate of their intensity. The background noise was estimated by using the rms of the deviation of a section of the spectrum with no lines. The response of the spectrometer and imaging system was derived from the spectra of the deuterium standard lamps taken alongside each HCL spectrum by dividing the measured lamp

Table 4
Semiempirical lifetimes for Levels of the $3d^4 4p$ Configuration

Term	J	Level Value (cm^{-1})	Lifetime (This Work)	Lifetime (Kurucz 2016)	Lifetime[a] (Average) (ns)	Residual[b] (%)	Previous[c] (ns)
$(a\ ^3P)4p\ y\ ^4D^\circ$	0.5	63801.7500	4.3	4.3	4.3	4.2	...
	1.5	64061.688	4.2	4.2	4.2	4.1	...
	2.5	64448.7503	4.1	4.1	4.1	1.2	...
	3.5	64924.4609	4.0	4.0	4.0	1.3	...
$(a\ ^3F)4p\ z\ ^4G^\circ$	2.5	65156.4895	4.7	4.8	4.7	2.9	...
	3.5	65256.8513	4.8	4.9	4.8	2.7	...
	4.5	65383.9035	4.8	5.0	4.9	1.5	...
	5.5	65709.4418	4.4	4.5	4.4	0.3	4.3 (0.6)
$(^3H)4p\ z\ ^4I^\circ$	4.5	65217.5070	4.2	4.4	4.3	2.2	4.0 (0.5)
	5.5	65419.5155	4.1	4.3	4.2	2.1	4.4 (0.5)
	6.5	65617.9458	4.0	4.3	4.2	1.1	...
	7.5	65812.6491	4.0	4.3	4.1	0.0	4.4 (0.5)
$(^3H)4p\ z\ ^2G^\circ$	3.5	65542.8987	5.5	5.2	5.4	3.6	...
	4.5	65680.0091	5.3	5.0	5.1	1.2	...

Notes.
[a] Lifetimes are an unweighted average of Kurucz (2016) and this work. One standard uncertainties of the semiempirical lifetimes are estimated as 10%.
[b] Sum of BFs for all calculated lines that were not observed in our spectra.
[c] Previously measured lifetime from Engman et al. (1975) with uncertainty in parenthesis.

spectrum by the known radiance of the lamp. They are shown in Figure 2. The line intensities of the Cr II lines were then obtained by dividing the observed intensities by this response. The BFs were combined with either measured lifetimes from Gurell et al. (2010) or semiempirical lifetimes described in Section 4.1.

4.1. Level Lifetimes

Table 3 shows a comparison of lifetimes from these two calculations with experimental values from Gurell et al. (2010). The uncertainties of Gurell et al. (2010) range from 7% to 13%. The levels from Gurell have similar excitations to our levels of interest and are from the same configuration. All but two of the 14 calculated lifetimes are within one experimental standard deviation of the the experimental lifetime, and all values are within two standard deviations. From this comparison, we assign an uncertainty of 10% to the semiempirical lifetimes, similar to that of the experimental lifetimes. The calculations of Tayal & Zatsarinny (2020) were also examined, but the lifetimes are systematically 14% shorter than the experimental ones.

The semiempirical lifetimes we have used for our transition probabilities are an unweighted average of the Kurucz (2016) and the lifetimes from this work, and are given in Table 4. The final column contains some previously measured lifetimes from Engman et al. (1975) that have uncertainties larger than 10%. Since the uncertainties of these lifetimes are greater than our estimated calculated lifetime uncertainties, we have not used them for deriving transition probabilities.

4.2. Branching Fractions and Uncertainties

The spectra were analyzed with the Python script PYBRANCH.PY (Nave et al. 2023), which computes a weighted average BF for each line from the integrated intensities and S/N ratios, and combines them with the level lifetime to obtain the transition probability. The program outputs the calibrated intensities and S/N ratios for all the lines observed from a particular upper level in each spectrum. The user then chooses one line to use as a reference to put all of the intensities on the same scale. If the reference line is not observed in a particular spectrum, the intensity scale of that spectrum can be set by using a normalization factor calculated from a strong transfer line that is observed in both that spectrum and other spectra that can be calibrated from the reference line (see Section 3.2.4 of Sikström et al. 2002). The program uses our calculated transition probabilities for lines that have not been observed to calculate a residual BF, comprising the sum of BFs for all lines in our calculations that were not observed in our spectra. This is shown in the last column of Table 3 and the seventh column of Table 4.

The calculation of the BF and its uncertainty is based on the analysis of Sikström et al. (2002). All uncertainties are one standard uncertainty. The following components of uncertainty are included in the PYBRANCH.PY script:

1. The statistical uncertainty $U_{\rm stat}$ of the line intensity is estimated from Equation (10) of Sikström et al. (2002) as

$$U_{\rm stat} = \frac{\alpha_Y}{({\rm S/N})\sqrt{n}} \quad (4)$$

where n is the number of points per FWHM of the line profile. The lineshape parameter, α_Y, varies from 1.41 ± 0.04 for a Gaussian line to 1.6 ± 0.04 for a Lorentian lineshape, and for simplicity a value of $\alpha_Y = 1.5$ was used.
2. The uncertainty with which the response of the spectrometer and imaging system can be measured is estimated from repeated observations of the calibration lamp on the same day. The maximum discrepancy in the relative response for these runs is 15%. Assuming this represents the extremes of a rectangular probability distribution, this results in an estimated standard relative uncertainty of $15\%/(2\sqrt{3}) = 4.3\%$ (Taylor & Kuyatt 1994; Section 4.6). This is added in quadrature to the 3.5% calibration uncertainty of the standard lamp to give an uncertainty in the calibration of 5.6%. We assumed this discrepancy is roughly linear with wavenumber. As noted

in Section 3.2.1 of Sikström et al. (2002), applying this uncertainty directly to each line would be an overestimate, as lines close together in wavenumber will have a much smaller uncertainty in the calibration than lines well separated in wavenumber. We thus multiplied the 5.6% uncertainty by a factor of $\Delta\sigma/W_\sigma$, where $\Delta\sigma$ is the separation of the line from the strongest line from the upper level of interest, and W_σ is the total width of the observed calibration spectrum.

3. The uncertainty of strong lines from each level in each spectrum is limited to a minimum of 6% to ensure that strong lines receive similar weighting in the average. This ensures that small systematic errors in the calibration do not have a significant influence on the results. The 6% minimum uncertainty was taken from the estimated calibration uncertainty and applied after combining the calibration and statistical uncertainties in quadrature.
4. The inverse square of the uncertainty derived from items 1–3 of the line in each spectrum was applied as a weighting factor to calculate the BF for each spectral line. The uncertainty of the BF is then derived from the first two terms in Equation (7) of Sikström et al. 2002.
5. In many cases, the reference line used to put the intensities in different spectra on the same scale is not seen in one or more spectra. A transfer line is then chosen that is observed with adequate S/N in both the spectrum without the reference line and in at least one spectrum containing the reference line. This line is used to calculate a normalizing factor f. The uncertainty of this normalizing factor $u(f)$ is derived from the weighted average of the quadrature sum of the uncertainty of the reference line $u(I_{\mathrm{ref},j})$ in each normalized spectrum, j, and the uncertainty of the transfer line $u(I_{\mathrm{trans},j})$ in each normalized spectrum:

$$u(f) = \Sigma_j \sqrt{u(I_{\mathrm{trans},j})^2 + u(I_{\mathrm{ref},j})^2}\,. \tag{5}$$

The uncertainty of the normalizing factor is added in quadrature to the uncertainty of each line in spectrum not containing the reference line.

6. The residuals in the last column of Table 3 and column (7) of Table 4 are applied as a correction to the summed intensities in Equation (1) before calculating the BF and transition probability. The relative uncertainty of the residuals is estimated to be 50%, as in Section 3.3 of Sikström et al. (2002). As noted in Sikström et al. (2002), its influence on the uncertainties of the measured lines is small provided that the residuals themselves are small.

4.3. Treatment of Blended Lines

Several lines in our spectra are a blend of two or more transitions. Two techniques were used to determine the intensities of the individual transitions of these lines. In some cases, the Cr II line of interest is blended with a Cr I line, and Cr I lines are either very weak or absent in the Penning spectrum (#7 in Table 1). Hence the measurement of the line intensity was taken solely from spectrum 7.

In other cases, the line is a blend of two Cr II transitions. Here, the proportion of each transition contributing to the spectral line was estimated from the center-of-gravity wavenumber of the line σ_{cog} and the Ritz wavenumbers of the two transitions σ_a and σ_b, taken from Sansonetti & Nave (2014).

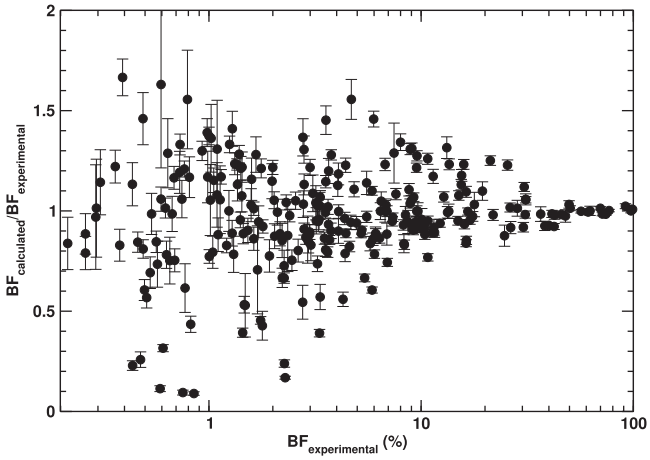

Figure 3. Comparison of our experimental and calculated branching fractions. The error bars are the one standard uncertainty of the experimental branching fractions and do not include estimated uncertainties on the calculated values. The branching fraction ratios and values used to create this plot are available as data behind the figure in the online version of this article.

(The data used to create this figure are available.)

The center of gravity of the transition is

$$\sigma_{\mathrm{cog}} = \frac{I_a\sigma_a + (I_t - I_a)\sigma_b}{I_t} \tag{6}$$

where I_a is the intensity of the transition of interest and I_t is the total intensity of the spectral line. Rearranging Equation (6) gives the corrected intensity for the transition of interest, I_a:

$$I_a = \frac{I_t(\sigma_{\mathrm{cog}} - \sigma_b)}{\sigma_a - \sigma_b}. \tag{7}$$

The contribution of the center of gravity to the uncertainty was estimated by applying the law of propagation of uncertainty from Equation (A-3) in Taylor & Kuyatt (1994) to Equation (7), using the Python uncertainty package. The principal components of uncertainty for strong lines are the uncertainties of the Ritz wavenumbers of the two transitions and the uncertainty of the wavenumber of the observed line. This technique is thus only usable if the wavenumbers have small uncertainties ($<0.005\,\mathrm{cm}^{-1}$), as the uncertainty can approach 50% or more if one wavenumber has a larger uncertainty. However, this can be reduced by using multiple spectra.

4.4. Comparison of Experimental and Calculated Branching Fractions

Figure 3 shows a comparison of our experimental and calculated BFs. For strong lines with a BF greater than 30%, the standard deviation is less than 5%. These strong lines dominate the lifetime of the upper energy level, so this finding is consistent with the good agreement between the experimental and calculated lifetimes. For weaker lines, however, the agreement between the experimental and calculated BFs gets poorer, with the standard deviation increasing to over 30% for weaker lines with a BF of less than 10%. These standard deviations have been used to assign an uncertainty of 10% to the calculated transition probabilities of lines with BFs greater than 20%, and 30% for lines with BFs less than 20%.

4.5. Transition Probabilities

Transition probabilities were derived for spectral lines from 14 levels using the lifetimes of Gurell et al. (2010) in Table 3 and 14 levels from the $(a\,^3P)4p\,y\,^4D$, $(a\,^3P)4p\,z\,^2S$, $(a\,^3F)4p\,z\,^4G$, $(^3H)4p\,z\,^4I$, and $(^3H)4p\,z\,^2G$ terms using the semiempirical lifetimes in Table 4. The one standard uncertainties of the semiempirical lifetimes are estimated to be 10%.

The transition probabilities are presented in Table 5. The Ritz wavenumber in column (2) was taken from Sansonetti & Nave (2014), as were the upper and lower level designations in columns (3) and (4) respectively, and upper and lower level values in columns (5) and (6) respectively. The Ritz air wavelength in column (1) was derived from the Ritz wavenumber using the five-parameter formula of Peck & Reeder (1972). The transition probabilities in column (9) were derived from the lifetimes in Tables 3 and 4 and the BF in column (7). Our calculated transition probabilities are given in column (11) with the uncertainties in column (12).

4.5.1. Notes on Individual Levels

$y\,^4D_{3/2}$. The line at 42,237.968 cm^{-1}, $a\,^4D_{1/2} - y\,^4D_{3/2}$, is a blend with the Cr I line $a\,^7S_3 - x\,^7P_2$. The Cr I line is almost absent in the Penning spectrum (spectrum 7 in Table 1), as seen by comparison with the other lines from the $x\,^7P_2$ level which are either weak or absent. The BF for this line was thus taken solely from spectrum 7.

$z\,^4G_{9/2}$. This level appears to be mixed with $z\,^2G_{9/2}$, giving a large number of transitions to doublet levels. Our semiempirical calculations show that the two largest LS terms contributing to this level are 29% $3d^4(^3F_4)^4G_{9/2}$ and 18% $3d^4(^3H_4)^2G_{9/2}$, the lowest purity of any of the levels in the present work.

$z\,^4G_{7/2}$. The line at 34,139.5259 cm^{-1}, $a\,^4F_{5/2} - z\,^4G_{7/2}$, is blended with a stronger Cr II line of higher excitation, $b\,^2G_{7/2} - x\,^2G_{7/2}$. The BF for the $a\,^4F_{5/2} - z\,^4G_{7/2}$ transition was thus derived from the center-of-gravity wavenumber as described in Section 4.3. The $a\,^4F_{5/2} - z\,^4G_{7/2}$ transition contributes between 39% for the lowest current run (spectrum 9 in Table 1) and 65% of the total intensity for the higher current runs (spectra 3 and 5 in Table 1). The uncertainties of the line wavenumber and of the energy levels of the two transitions are roughly 0.001 cm^{-1}, resulting in Ritz wavelength uncertainties of 0.0014 cm^{-1}. Hence the center-of-gravity technique increases the uncertainty of the resulting BF by only 5% to 10% in each spectrum and the final BF uncertainty is 1.9%.

$z\,^4I_{11/2}$. The line at 35,121.0 cm^{-1} is a blend between $a\,^4H_{11/2} - z\,^4I_{11/2}$ and $c\,^4H_{11/2} - w\,^4D_{11/}$. The former line has a small contribution to the total intensity and treatment using the center-of-gravity technique results in a large uncertainty. The experimental intensity was thus omitted from the calculation of the total BF and the branching fraction from our semiempirical calculations for this line was included in the residual.

$z\,^2G_{9/2}$. The line at 34,511.4336 cm^{-1} is a blend with a Cr I line. The Cr I line is weak in the Penning spectrum 7; hence the BF for this line was taken solely from this spectrum. The level is strongly mixed with $z\,^4G_{9/2}$, giving many transitions to quartet levels.

$y\,^4F_{5/2}$ and $y\,^4F_{3/2}$. The line at 27,328 cm^{-1} is a blend of $c\,^2F_{5/2} - y\,^4F_{3/2}$, at 27,328.3991 cm^{-1} and $c\,^2G_{7/2} - y\,^4F_{5/2}$ at 27,328.3584 cm^{-1}. It was only observed in the highest-current HCL spectrum number 8. Treatment using the center-of-gravity technique results in 70% of the line being assigned to $c\,^2F_{5/2} - y\,^4F_{3/2}$ and 30% to $c\,^2G_{7/2} - y\,^4F_{5/2}$, with an increased uncertainty of 10% for the former transition and 20% for the latter. This line is assigned to these two transitions in Gurell et al. (2010), and also to the transition $a\,^2G_{9/2} - z\,^4H_{7/2}$, with a transition probability of 3.3×10^6 s^{-1}. However, this third transition is unlikely to contribute significantly to the line at 27,328.4 cm^{-1}, as the transition probability in our semiempirical calculations is just 2.2×10^3 s^{-1}. It is not clear from Gurell et al. (2010) how the blend between the remaining transitions was treated, as the two transitions are too close together to be resolved in spectra of hollow cathode or Penning discharge sources. The transition probabilities for all three transitions in Gurell et al. (2010) are thus likely incorrect. Since their BFs for the transitions are less than 3%, their incorrect values will only have a small effect on the other results from the upper levels.

The line at 31,501.2568 cm^{-1} is blended with a neon line in spectrum 9. The line in this spectrum was thus discarded in the calculation of the BF and the calculated BF from our semiempirical calculations was used in the residual instead.

The line at 36,704.65 cm^{-1} is listed in Gurell et al. (2010) as $b\,^4P_{3/2} - y\,^4F_{5/2}$, with a Ritz wavenumber of 36,704.7082 cm^{-1} using the energy levels of Sansonetti et al. (2012), and a transition probability of 5.7×10^6 s^{-1} from our semiempirical calculations. The line is listed as $b\,^4G_{11/2} - y\,^2H_{11/2}$ in Sansonetti et al. (2012), with a Ritz wavenumber of 36,704.656 cm^{-1} and a transition probability of 1×10^8 s^{-1} from our semiempirical calculations, much stronger than the transition listed in Gurell et al. (2010). This line appears with an S/N of 675 at 36,704.659 cm^{-1} in spectrum 7, very close to the Ritz wavenumber from Sansonetti et al. (2012). We thus conclude that this line was misidentified in Gurell et al. (2010).

$y\,^4G_{11/2}$. The line at 34,514.819 cm^{-1} is a blend between $b\,^4F_{9/2} - y\,^4G_{11/2}$ and $b\,^2I_{11/2} - 3d^4(^1I)4p\,^2I_{13/2}$. The former transition contributes roughly 25% to the total intensity of the line and leads to an increased uncertainty of 12% for the BF. The line was identified as $b\,^4F_{9/2} - y\,^4G_{11/2}$ in Gurell et al. (2010), with a transition probability of 3.56×10^7, slightly larger than our value of 2.8×10^7.

4.6. Comparison with Previous Results

Figure 4 shows a comparison of all 72 lines with a transition probability above 10^7 s^{-1} with those of Gurell et al. (2010). While there is considerable scatter in the comparison, the transition probabilities of Gurell et al. (2010) are an average of 77% larger than ours for wavenumbers above 45,000 cm^{-1}. The most likely reason for this is a problem in the radiometric calibration of one or both sets of spectra. Our spectra show good consistency between spectra taken under different conditions, ranging from low-current HCL spectra taken at a current of 20 mA to high-current HCL spectra taken at a current of 2 A. Good consistency is also shown with spectra calibrated using different deuterium lamps, and with spectra taken several years apart. An example is shown in Table 6 for five transitions from the level $3d^5(a\,^3F)4p\,y\,^4F_{9/2}$, spanning wavenumbers from 34,594.29 to 47,424.539 cm^{-1}. All our lines in the table have S/Ns greater than 20 and were multiplied by a common factor so that the BR of the line at 46,936.445 cm^{-1} was 1000. The BRs in our spectra agree to 5%, but differ from those of Gurell et al. (2010) by roughly a factor of 2 between the lines

Table 5
Transition Probabilities in Cr II

Ritz Air[a] Wavelength (nm)	Ritz[a] Wavenumber (cm^{-1})	Lower Level[b] Designation	Upper Level[b] Designation	Lower Level Value (cm^{-1})	Upper Level Value (cm^{-1})	BF[c] (%)	Unc.[d] (%)	A[e] (10^6 s^{-1})	Unc.[d] (10^6 s^{-1})	A_{calc}[f] (10^6 s^{-1})	Unc.[d] (10^6 s^{-1})
208.915314	47,851.0657	3d4.(5D).4 s a 4D 1/2	3d4.(a 3F).4p z 2D* 3/2	19,528.2293	67,379.2950	3.1	0.3	10.0	1.3	10	3
209.331749	47,755.8848	3d4.(5D).4 s a 4D 3/2	3d4.(a 3F).4p z 2D* 5/2	19,631.2058	67,387.0906	2.81	0.15	9.0	1.0	12	3
210.036833	47,595.5901	3d4.(5D).4 s a 4D 5/2	3d4.(a 3F).4p y 4F* 7/2	19,797.8594	67,393.4495	3.00	0.10	10.3	1.1	13	4
210.064902	47,589.2312	3d4.(5D).4 s a 4D 5/2	3d4.(a 3F).4p z 2D* 5/2	19,797.8594	67,387.0906	1.09	0.20	3.5	0.7	4.5	1.3
210.300526	47,535.9180	3d4.(5D).4 s a 4D 5/2	3d4.(3H).4p y 4G* 7/2	19,797.8594	67,333.7774	1.02	0.17	3.9	0.8	4.2	1.3
210.794533	47,424.5288	3d4.(5D).4 s a 4D 7/2	3d4.(a 3F).4p y 4F* 9/2	20,024.0117	67,448.5405	4.41	0.13	15.2	1.5	19	6
212.752804	46,988.0637	3d4.(5D).4 s a 4D 7/2	3d4.(a 3F).4p y 4F* 5/2	20,024.0117	67,012.0754	1.98	0.15	5.4	0.7	5.4	1.6

Notes.
[a] Ritz wavenumber taken from Sansonetti & Nave (2014). Ritz air wavelength calculated from wavenumber using five-parameter formula of Peck & Reeder (1972).
[b] Upper and lower designations taken from Sansonetti & Nave (2014). The asterisk denotes odd parity.
[c] Experimental branching fraction.
[d] One standard uncertainty of the previous column.
[e] Transition probability derived from experimental BF and lifetime.
[f] Calculated transition probability from this work.

(This table is available in its entirety in machine-readable form.)

Table 6
Comparison of BRs in Our Spectra with Those of Gurell et al. (2010), and with Our Calculations, for Lines from the $y\,^4F_{9/2}$ Level

File Name[a]	Current (A)	Calibration Lamp	BR with Respect to 46,936.445 cm^{-1}			
			47,424.53[b]	46,929.27[b]	36,229.208[b]	34,594.292[b]
4	1.5	BR0065	0.28	0.48	2.8	1.03
5	1.5	BR0065	0.29	0.47	2.7	0.97
6	0.7	BR0065	0.28	0.44	2.7	…
9	0.02	V0236	…	…	2.8	1.05
Gurell[c]	...	...	0.27	0.44	1.1	0.51
This work[d]	...	...	0.30	0.38	2.3	0.82

Notes. All BRs are with respect to the transition at 46,936.445 cm^{-1}.
[a] Number of file in Table 1.
[b] Wavenumber of the line in cm^{-1}.
[c] BR from Gurell et al. (2010).
[d] BR from our semiempirical calculations.

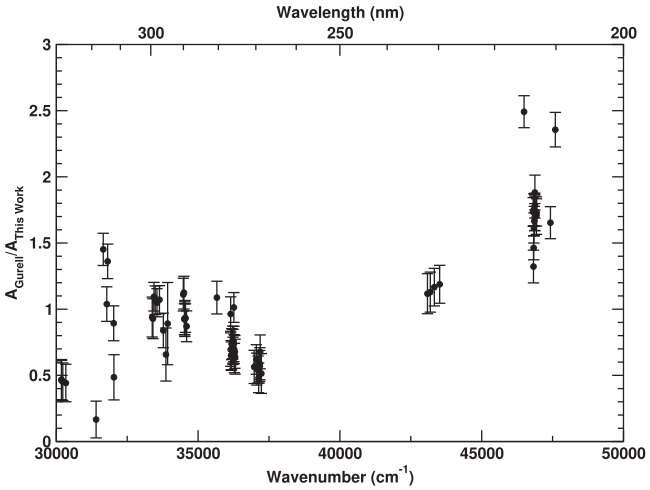

Figure 4. Comparison of the transition probabilities from this work, $A_{Thiswork}$, with those of Gurell et al. (2010), A_{Gurell}. The transition probabilities and wavenumbers used to create this plot are available as data behind the figure in the online version of this article.

(The data used to create this figure are available.)

around 35,000 cm^{-1} and those around 47,000 cm^{-1}. Our BRs agree much better with the values from our semiempirical calculations, shown in the last line of the table.

5. Conclusions

We have measured transition probabilities for 268 lines of Cr II covering the wavelength range 208 to 414 nm, by combining archival measurements of BFs using FT spectroscopy with either measured lifetimes from Gurell et al. (2010) or lifetimes from atomic structure calculations. The calculated and measured lifetimes agree within 10% and we have adopted this value as the uncertainty of calculated lifetimes. The uncertainties of the transition probabilities range from 10% to 26%. All lines are from 28 levels from the $3d^4 4p$ configuration covering energy level values from 63,600 to 67,448 cm^{-1}.

Acknowledgments

This work was partially supported by NASA under the interagency agreement 80HQTR18T0031. J.S. was supported by a NIST Summer Undergraduate Research Fellowship. J.L. performed the work as part of the NIST Summer High School Intern Program. Spectra 1–7 in Table 1 used in this paper were taken in 2000 by Andreas Knoche and Ulf Griesmann as NIST Guest Researchers.

ORCID iDs

Jacob W. Ward https://orcid.org/0000-0002-5841-0649
Jacqueline J. Li https://orcid.org/0000-0002-7849-5483
Gillian Nave https://orcid.org/0000-0002-1718-9650
Peter H. M. Uylings https://orcid.org/0000-0001-6876-2472

References

Bergeson, S. D., & Lawler, J. E. 1993, ApJ, 408, 382
Bouazza, S., Palmeri, P., & Quinet, P. 2018a, ADNDT, 120, 338
Bouazza, S., Quinet, P., & Palmeri, P. 2018b, ADNDT, 120, 323
Castelli, F., Cowley, C. R., Ayres, T. R., Catanzaro, G., & Leone, F. 2017, A&A, 601, A119
Danzmann, K., Günther, M., Fischer, J., & Kock, M. 1988, ApOpt, 27, 4947
Engman, B., Gaupp, A., Curtis, L. J., & Martinson, I. 1975, PhyS, 12, 220
Engström, L., Lundberg, H., Nilsson, H., Hartman, H., & Bäckström, E. 2014, A&A, 570, A34
Froese Fischer, C., Gaigalas, G., Jönsson, P., & Bieroń, J. 2019, CoPhC, 237, 184
Fuhr, J. R., & Wiese, W. L. 2005, in CRC Handbook of Chemistry and Physics, ed. D. R. Lide (86th ed.; Boca Raton, FL: CRC Press)
Griesmann, U., Kling, R., Burnett, J. H., & Bratasz, L. 1999, Proc. SPIE, 3818, 180
Gurell, J., Nilsson, H., Engström, L., et al. 2010, A&A, 511, A68
Hansen, J. E., Uylings, P. H. M., & Raassen, A. J. J. 1988, PhyS, 37, 664
Heise, C., Hollandt, J., & Kling, R. 1994, ApOpt, 33, 5111
Kling, R., & Griesmann, U. 2000, ApJ, 531, 1173
Kramida, A., Ralchenko, Y., Reader, J. & NIST ASD Team 2022, NIST Atomic Spectra Database, v5.9 (Gaithersburg, MD: National Institute of Standards and Technology)
Kurucz, R. 2016, Atomic spectral line database from CD-ROM 23 of R. L. Kurucz (Cambridge, MA: Smithsonian Astrophysical Observatory) http://kurucz.harvard.edu
Lawler, J. E., Sneden, C., Cowan, J. J., Hartog, E. A. D., & Wood, M. P. 2017a, CaJPh, 95, 783
Lawler, J. E., Sneden, C., Nave, G., et al. 2017b, ApJS, 228, 10
Morton, D. C. 2003, ApJS, 149, 205
Musielok, J., & Wujec, T. 1979, A&AS, 38, 119
Nave, G., Griesmann, U., Brault, J. W., & Abrams, M. C., 2015 Xgremlin: A code for analyzing interferograms and spectra from Fourier transform spectrometers, Astrophysics Source Code Library, ascl:1511.004
Nave, G., Ward, J., Li, J., & Zuckman, N., 2023 pybranch: Calculate experimental branching fractions and transition probabilities from atomic spectra, Astrophysics Source Code Library, ascl:2306.057
Nilsson, H., Ljung, G., Lundberg, H., & Nielsen, K. E. 2006, A&A, 445, 1165
Peck, E. R., & Reeder, K. 1972, JOSA, 62, 958
Pinnington, E. H., Ji, Q., Guo, B., et al. 1993, CaJPh, 71, 470
Raassen, A. J. J., & Uylings, P. H. M. 1996, PhST, T65, 84

Sansonetti, C. J., & Nave, G. 2014, ApJS, 213, 28
Sansonetti, C. J., Nave, G., Reader, J., & Kerber, F. 2012, ApJS, 202, 15
Schade, W., Mundt, B., & Helbig, V. 1990, PhRvA, 42, 1454
Sikström, C. M., Nilsson, H., Litzén, U., Blom, A., & Lundberg, H. 2002, JQSRT, 74, 355
Tayal, S. S., & Zatsarinny, O. 2020, ApJ, 888, 10
Taylor, B., & Kuyatt, C. 1994, Guidelines for Evaluating and Expressing the Uncertainty of NIST Measurement Results, NIST Technical Note 1297, National Institute of Standards and Technology
Uylings, P., & Raassen, T. 2019, Atoms, 7, 102